Proceedings of the 1991 ICHMT International Symposium on Heat and Mass Transfer in Biomedical Engineering, Editors: K.Diller, A.Shitzer and S.Sideman, Hemisphere Publishing Corporation, Athens, Greece, September 2-6, 1991.

FREEZING UNDER THE INFLUENCE OF A MAGNETIC FIELD: COMPUTER SIMULATION

Branko Kosovic , Graduate Student
George S. Dulikravich, Associate Professor
Department of Aerospace Engineering, The Pennsylvania State University
University Park, PA 16802, USA
and
Seungsoo Lee, Postdoctoral Fellow presently with
Agency for Defense Development, Daejon, Korea

ABSTRACT

A complete mathematical model and an accompanying computer program have been developed for the computational simulation of a steady laminar flow of an incompressible fluid with strong heat transfer and a strong superimposed magnetic field. Boussinesq approximation and temperature-dependent physical properties of the fluid including latent heat of phase change were incorporated. The computed example configurations involve two-dimensional straight and U-shaped channels and a passage of an arbitrary shape. This formulation simultaneously predicts detailed velocity and temperature fields for the moving coolant while capturing the forming solid phase by using a single computer code. The same code can simulate the reverse process of thawing or melting of the solid phase. It was found that the presence of an external steady magnetic field: a) diminishes flow field vorticity, b) causes higher velocity gradients within the boundary layers, and c) inhibits the solid phase accretion rate and the total amount of solid accrued.

1. INTRODUCTION

During a controlled freezing process (Dulikravich and Hayes, 1988) of a large amount of living tissue and especially in the case of perfusion cooled organs, it is very important to fully understand the process of ice accretion on the walls of the passages. The accumulated ice effectively reduces and deforms the cross sectional area of the passage and causes significant local variations in pressure and flow field shear stresses. Eventually, the ice completely fills the passage at certain locations thus blocking the main flow and creating isolated pockets of undercooled fluid. Further freezing of this fluid creates significant residual stresses in the frozen material. During the cooling or thawing process, secondary flows are generated due to strong buoyancy forces. These processes cannot be effectively controlled in the case of strong heat transfer, except if influenced by a global body force of certain type. One such body force is the general electromagnetic Lorentz force which is created in any electrically conducting fluid when either a magnetic field or an electric potential field is applied. It has been shown (Lee and Dulikravich, 1991a; Lee and Dulikravich, 1991b; Lee, Dulikravich and Kosovic, 1991a; Dulikravich, Kosovic and Lee, 1991) that the magnetic field can eliminate vorticity from the flow field, while the electric field can enhance it (Lee, Dulikravich and Kosovic, 1991b). During the perfusion freezing of organs we usually work with electrically conducting fluids. They are conducting either because of the presence of iron atoms (blood hemoglobin), salts (saline coolant solutions), or acids (DMSO and similar coolants). Thus, if a relatively strong magnetic field is applied to an organ perfused by such a liquid, the flow field will respond (Heiser, 1964; Ievlev and Levy, 1989; Ozoe and Okada, 1989) and the freezing front could be manipulated (Vives, 1989; Dulikravich, Kosovic and Lee, 1991). The applied magnetic field can be oscillatory, travelling, or steady. In this work we have formulated the entire problem as time-dependent and three-dimensional although our computational results will be for steady two-dimensional situations only.

2. ANALYTICAL MODEL

Maxwell's equations can be written in Cartesian tensor notation as

$$\varepsilon_{ijk} H_{k,j} = J_i \tag{1}$$

$$H_{i,t} = -\frac{1}{\mu} \varepsilon_{ijk} E_{k,j} \tag{2}$$

$$H_{i,i} = 0. \tag{3}$$

The relationship between an induced electric current, J_i, an electric field, E_i, and an externally applied magnetic field, H_i, in a moving media is given by Ohm's law

$$J_i = \sigma \left(E_i + \mu \varepsilon_{ijk} v_j H_k\right) \tag{4}$$

where σ, μ, and v_j are the coefficient of electric conductivity, coefficient of magnetic permeability, and fluid velocity vector, respectively. From equations (1-3) we can derive the magnetic field transport equation (Chandrasekhar, 1961; Pai, 1962; Stuetzer, 1962; Jeffrey, 1966; Lee and Dulikravich, 1991a) as

$$H_{i,t} - \left(v_j H_i - v_i H_j\right)_{,j} = \frac{1}{\mu\sigma} H_{i,jj}. \tag{5}$$

Under the assumption that the fluid is a continuum, the flow can be modeled with a system of compressible flow Navier-Stokes equations. Only incompressible fluid flow will be considered in this work while accounting for thermal buoyancy via Boussinesq approximation in the form which is valid even when fluid properties vary as a function of temperature (Gray and Giorgini, 1976). The extended Boussinesq approximation can be derived by starting from the full Navier-Stokes equations for a compressible fluid flow under the influence of an externally applied steady magnetic field (Stuetzer, 1962; Lee and Dulikravich, 1991a).

$$\rho_{,t} + \left(\rho v_i\right)_{,i} = 0 \tag{6}$$

$$\left(\rho v_i\right)_{,t} + \left(\rho v_i v_j\right)_{,j} = -p_{,i} - \rho g_i + \left(\eta \left(v_{i,j} + v_{j,i}\right) + \zeta v_{k,k} \delta_{ij}\right)_{,j} + \mu \varepsilon_{ijk}\varepsilon_{jlm} H_{m,l} H_k \tag{7}$$

where $\mu \varepsilon_{ijk} J_j H_k$ is the Lorentz force due to the magnetic field, ρ is the fluid density, p is the pressure, g_i is the acceleration due to gravity, η and ζ are the coefficients of shear and secondary viscosity, respectively, while δ_{ij} is the Kronecker delta. The energy conservation equation is given as

$$\left(\rho c_v T\right)_{,t} + \left(\rho c_v v_i T\right)_{,i} = \left(kT_{,i}\right)_{,i} - p\, v_{i,i} + \frac{J_i J_i}{\sigma} + \left(\eta \left(v_{i,j} + v_{j,i}\right) + \zeta v_{k,k} \delta_{ij}\right) v_{i,j} \tag{8}$$

where c_v is the coefficient of specific heat at constant volume, k is the heat conduction coefficient, and $\frac{J_i J_i}{\sigma}$ is the Joule heating resulting from the induced electric current, J_i. The viscous dissipation function is defined as $\Phi = \tau_{ij} v_{i,j}$. Fluid density and coefficients of specific heat, viscosity and heat conduction can be expressed as general functions of temperature (Gray and Giorgini, 1976):

$$\rho = \rho_o \rho'(\theta) \qquad c_p = c_{po} c_{po}'(\theta) \qquad c_v = c_{vo} c_{vo}'(\theta) \tag{9}$$

$$\eta = \eta_o \eta'(\theta) \qquad \zeta = \eta_o \zeta'(\theta) \qquad k = k_o k'(\theta) \tag{10}$$

where the primed values denote functions of non-dimensional temperature, θ. The entire set of partial differential equations can be non-dimensionalized by introducing the relations

$$v_i^* = \frac{v_i}{v_o} \qquad x_i^* = \frac{x_i}{l_o} \qquad t^* = \frac{t\, v_o}{l_o} \qquad p^* = \frac{p}{\rho_o v_o^2} \qquad g^* = \frac{g_i}{g} \tag{11}$$

$$\Phi^* = \frac{\Phi}{\eta_o v_o^2/l_o^2} \qquad H_i^* = \frac{H_i}{H_o} \qquad \theta = \frac{\Delta T}{\Delta T_o} \qquad e^* = \frac{e}{c_{po}\, \Delta T_o} \tag{12}$$

where T_c is the temperature of the cold wall and T_h is the temperature of the hot wall, so that $\Delta T = T - T_c$, and $\Delta T_o = T_h - T_c$. With the following non-dimensional groups

Reynolds number $\mathrm{Re} = \dfrac{\rho_o v_o l_o}{\eta_o}$ Froude number $\mathrm{Fr}^2 = \dfrac{v_o^2}{g\, l_o}$

Grashof number $\mathrm{Gr} = \dfrac{\rho_o^2\, \alpha\, g\, l_o^3\, \Delta T_o}{\eta_o^2}$ Eckert number $\mathrm{Ec} = \dfrac{v_o^2}{c_{po}\, \Delta T_o}$

Prandtl number $\mathrm{Pr} = \dfrac{\eta_o c_{po}}{k_o}$ Magnetic Prandtl number $\mathrm{Pm} = \dfrac{\mu\, \sigma\, \eta_o}{\rho_o}$

Hartmann number $\mathrm{Ht} = \mu\, l_o\, H_o \left(\dfrac{\sigma}{\eta_o}\right)^{1/2}$ Magnetic Reynolds number $\mathrm{Rm} = \mathrm{Re}\, \mathrm{Pm}$

Magnetic Mach number $\mathrm{Mm}^2 = \dfrac{\mathrm{ReRm}}{\mathrm{Ht}^2} = \dfrac{\rho_o v_o^2}{\mu\, H_o^2}$ (13)

the conservation laws in non-dimensional form become

$$\rho'_{,t} + \left(\rho'\, v_i^*\right)_{,i} = 0 \tag{14}$$

$$\left(\rho' v_i^*\right)_{,t} + \left(\rho' v_i^* v_j^*\right)_{,j} = -\, p_{,i}^* - \frac{1}{\mathrm{Fr}^2} \rho'\, g_i^* + \frac{1}{\mathrm{Re}} \left[\eta' \left(v_{i,j}^* + v_{j,i}^*\right)\right]_{,j} + \frac{1}{\mathrm{Re}} \left(\zeta'\, v_{j,j}^*\right)_{,i} + \frac{1}{\mathrm{Mm}^2} \varepsilon_{ijk}\, \varepsilon_{jlm} H_{m,l}^* H_k^* \tag{15}$$

$$(\rho' e^*)_{,t} + (\rho' e^* v_i^*)_{,i} = \frac{1}{RePr}(k' \theta_{,i})_{,i} - Ec\, p^* v_{i,i}^* + \frac{Ec}{Mm^2 Rm} \varepsilon_{ijk}\varepsilon_{ilm} H_{k,j}^* H_{m,l}^* + \frac{Ec}{Re} \Phi^* \quad (16)$$

$$H_{i,t}^* - (v_j^* H_i^* - v_i^* H_j^*)_{,j} = \frac{1}{Rm} H_{i,jj}^* \quad (17)$$

The non-dimensional density ρ' can be expanded in a Taylor series while retaining only the first order term

$$\rho' = 1 - \alpha \Delta T = 1 - \alpha^* \theta \quad (18)$$

where

$$\alpha^* = \frac{\partial \rho'}{\partial \theta} = \frac{\Delta T_o \rho_o}{\rho_o \Delta T_o} \frac{\partial \rho'}{\partial \theta} = \frac{\Delta T_o}{\rho_o} \frac{\partial \rho}{\partial T} = \Delta T_o \alpha \quad (19)$$

It can be assumed that the coefficient of thermal expansion, α, is constant in the range of temperatures which are of interest in a particular case. When the term $(\Delta T_o \alpha) \ll 1$, equations more general than what is known as Boussinesq approximation can be derived for the fluid with non-constant properties (Gray and Giorgini, 1976). Thus, the system of equations (14-17) can be reduced to

$$v_{i,i}^* = 0 \quad (20)$$

$$v_{i,t}^* + (v_i^* v_j^*)_{,j} = \frac{1}{Re}(\eta' v_{i,j}^*)_{,j} - p_{,i}^* - \frac{1}{Fr^2} g_i^* + \frac{\alpha^* \theta}{Fr^2} g_i^* + \frac{1}{Mm^2} \varepsilon_{ijk}\varepsilon_{jlm} H_{m,l}^* H_k^* \quad (21)$$

$$c_p' \theta_{,t} + c_p' (v_i^* \theta)_{,i} = \frac{1}{RePr}(k' \theta_{,i})_{,i} + \frac{Ec}{Mm^2 Rm} \varepsilon_{ijk}\varepsilon_{ilm} H_{k,j}^* H_{m,l}^* + \frac{Ec}{Re} \Phi^{*(i)} \quad (22)$$

$$H_{,t}^* - (v_j H_i^* - v_i H_j^*)_{,j} = \frac{1}{Rm} H_{i,jj}^* \quad (23)$$

where $\Phi^{*(i)}$ is the energy dissipation function for incompressible viscous flow.

$$\Phi^{*(i)} = \eta' (v_{i,j}^* + v_{j,i}^*) v_{i,j}^* \quad (24)$$

For incompressible flows $c_p = c_v$. Thus, it follows that $de = c_v\, dT = c_p\, dT$. In the case of a liquid/solid mixture the enthalpy per unit mass of the mushy region becomes

$$dh = c_p\, dT + L\, dS \quad (25)$$

where L is the latent heat (enthalpy of solid/liquid phase change) and S is the volumetric fraction of the solid phase. Then

$$v_i h_{,i} = c_p v_i T_{,i} - L\, v_i S_{,i} = (c_p - L S_{,T})\, v_i T_{,i} \quad (26)$$

Let $c_{pe} = c_p - L S_{,T}$ be an equivalent specific heat so that

$$c_{pe} = c_{po}\, c_{pe}' = c_{po}\left(c_p' - \frac{L\, S_{,\theta}\, \theta_{,T}}{C_{po}}\right) \tag{27}$$

where S could be an arbitrary function of θ and c_{pe}' is the non-dimensional equivalent specific heat. This approach is called the "enthalpy method" (Porier and Salcudean, 1986).For clarity, asterisk symbols will be dropped in the following formulas. After introducing $\frac{Gr\,\theta}{Re^2}$ instead of $\frac{\alpha^*\theta}{Fr^2}$ in equation 21 and the non-dimensional equivalent specific heat c_{pe}' in equation 22, the non-dimensional equations (20-23) become

$$v_{i,i} = 0 \tag{28}$$

$$v_{i,t} + (v_i\, v_j)_{,j} = \frac{1}{Re}(\eta'\, v_{i,j})_{,j} - \tilde{p}_{,i} + \frac{Gr\,\theta}{Re^2}\, g_i + \frac{Ht^2}{RmRe}\,(H_i\, H_k)_{,k} \tag{29}$$

$$\theta_{,t} + v_i\, \theta_{,i} = \frac{1}{RePr\, c_{pe}'}(k'\, \theta_{,i})_{,i} + \frac{EcHt^2}{Rm^2 Re\, c_{pe}'}\varepsilon_{ijk}\varepsilon_{ilm}H_{k,j}H_{m,l} \tag{30}$$

$$H_{,t} - (v_j\, H_i - v_i\, H_j)_{,j} = \frac{1}{Rm}\, H_{i,jj} \tag{31}$$

It should be pointed out that the viscous dissipation $\Phi^{(i)}$ can be neglected from an order of magnitude analysis since, for example, for water with $c_{po} = 4179$ J/(kg K), $\rho_0 = 1003$ kg/m^3, $\eta_o = 0.0017$ kg/(m s) it follows that

$$\frac{\rho_o\, c_{pe}\, \frac{\partial T}{\partial t}}{\Phi^{(i)}} = \frac{\rho_o\, c_{pe}\, \Delta T_o\, v_o}{\eta_o\, \frac{v_o^2}{l_o^2}\, l_o} = \frac{Re}{Ec} = 2.46 \times 10^9\, \frac{\Delta T_o\, l_o}{v_o} \tag{32}$$

The combination of non-dimensional hydrostatic, hydrodynamic, and magnetic pressures is

$$\tilde{p} = p + \frac{\phi}{Fr^2} + \frac{1}{Mm^2} H_i H_i \tag{33}$$

where ϕ is the non-dimensional gravity potential defined as $g_i = \phi_{,i}$.

3. NUMERICAL ALGORITHM

Equations (28-31) represent a global system of coupled non-linear partial differential equations. The global system has been split in two subsystems in order to simplify programming. The Navier-Stokes equations (28-30) constitute the first subsystem and magnetic field transport equations (31) constitute the second subsystem. To integrate each subsystem, the explicit Runge-Kutta time stepping method (Jameson et al., 1981) was used in an alternating manner (Lee and Dulikravich, 1991a).

The general form of each subsystem is the same. The non-dimensional three-dimensional Navier-Stokes equations for incompressible flows in conservative form expressed in generalized curvilinear non-orthogonal coordinates are

$$\frac{\partial \tilde{Q}}{\partial t}+\frac{\partial \tilde{E}}{\partial \xi}+\frac{\partial \tilde{F}}{\partial \eta}+\frac{\partial \tilde{G}}{\partial \zeta}=D^2+\tilde{S} \tag{34}$$

where $\tilde{Q}$ is the solution vector and $\tilde{E}$, $\tilde{F}$ and $\tilde{G}$ are the flux vectors. The transformed source vector is denoted by $\tilde{S}$. Definitions of these vectors will be given for both systems of equations (Navier-Stokes and magnetic transport) separately. For the Navier-Stokes equations, the generalized vectors are defined as

$$\tilde{Q}=\frac{1}{J}\begin{bmatrix}\bar{p}/\beta\\ u\\ v\\ w\\ \theta\end{bmatrix} \qquad \tilde{E}=\frac{1}{J}\begin{bmatrix}U\\ Uu+\xi_x\bar{p}\\ Uv+\xi_y\bar{p}\\ Uw+\xi_z\bar{p}\\ U\theta\end{bmatrix} \qquad \tilde{F}=\frac{1}{J}\begin{bmatrix}V\\ Vu+\eta_x\bar{p}\\ Vv+\eta_y\bar{p}\\ Vw+\eta_z\bar{p}\\ V\theta\end{bmatrix}$$

$$\tilde{G}=\frac{1}{J}\begin{bmatrix}W\\ Wu+\zeta_x\bar{p}\\ Wv+\zeta_y\bar{p}\\ Ww+\zeta_z\bar{p}\\ W\theta\end{bmatrix} \qquad \tilde{S}=\begin{bmatrix}0\\ \tilde{d}_2\\ \tilde{d}_3\\ \tilde{d}_4\\ \tilde{d}_5\end{bmatrix} \qquad \tilde{D}=\frac{1}{Re}\begin{bmatrix}0\\ \eta'\\ \eta'\\ \eta'\\ k'/(Pr\,c_p')\end{bmatrix}^T \tag{35}$$

where $J=\dfrac{\partial(\xi,\eta,\zeta)}{\partial(x,y,z)}$ is the Jacobian determinant of the geometric transformation from physical Cartesian coordinates x, y, z into ξ, η, ζ computational space.

The system of equations given by (28-31) is not hyperbolic since there is no physical time derivative term in the mass conservation equation. Consequently, the system cannot be integrated simultaneously. In order to integrate the system simultaneously and obtain a steady state solution, an artificial compressibility (Chorin, 1967) term, $\dfrac{\partial}{\partial t}\left(\dfrac{\bar{p}}{\beta J}\right)$, has been added to the mass conservation equation (28). Here, β is an artificial compressibility coefficient, a user specified parameter that depends on the problem geometry, grid, flow parameters, etc. (Lee and Dulikravich, 1991c). In the steady state limit the artificial compressibility term tends to zero. Thus, it does not influence the steady state solution.

The source vector $\tilde{S}$ contains the influence of the ponderomotive force due to the magnetic field and the thermal buoyancy force. Its components are given as

$$\tilde{d}_2 = \frac{Ht^2}{RmRe}\left[\frac{\partial}{\partial\xi}\left(\frac{\hat{H}_\xi H_x}{J}\right) + \frac{\partial}{\partial\eta}\left(\frac{\hat{H}_\eta H_y}{J}\right) + \frac{\partial}{\partial\zeta}\left(\frac{\hat{H}_\zeta H_z}{J}\right)\right] + \frac{Gr\theta}{Re^2 J} e_\xi \tag{36}$$

$$\tilde{d}_3 = \frac{Ht^2}{RmRe}\left[\frac{\partial}{\partial\xi}\left(\frac{\hat{H}_\xi H_y}{J}\right) + \frac{\partial}{\partial\eta}\left(\frac{\hat{H}_\eta H_y}{J}\right) + \frac{\partial}{\partial\zeta}\left(\frac{\hat{H}_\zeta H_y}{J}\right)\right] + \frac{Gr\theta}{Re^2 J} e_\eta \tag{37}$$

$$\tilde{d}_4 = \frac{Ht^2}{RmRe}\left[\frac{\partial}{\partial\xi}\left(\frac{\hat{H}_\xi H_z}{J}\right) + \frac{\partial}{\partial\eta}\left(\frac{\hat{H}_\eta H_z}{J}\right) + \frac{\partial}{\partial\zeta}\left(\frac{\hat{H}_\zeta H_z}{J}\right)\right] + \frac{Gr\theta}{Re^2 J} e_\zeta \tag{38}$$

$$\tilde{d}_5 = \frac{1}{c_{pe}}\frac{EcHt^2 J}{RmRe^2}\left[\tilde{P}_1^2 + \tilde{P}_2^2 + \tilde{P}_3^2\right] \tag{39}$$

where H_x, H_y, H_z are the components of the magnetic field vector in Cartesian coordinates, e_ξ e_η, e_ζ are components of the unit vector in the direction of gravity force, and

$$\tilde{P}_1 = \frac{\partial}{\partial\xi}\left(\frac{H_z\xi_y - H_y\xi_z}{J}\right) + \frac{\partial}{\partial\eta}\left(\frac{H_z\eta_y - H_y\eta_z}{J}\right) + \frac{\partial}{\partial\zeta}\left(\frac{H_z\zeta_y - H_y\zeta_z}{J}\right) \tag{40}$$

$$\tilde{P}_2 = \frac{\partial}{\partial\xi}\left(\frac{H_x\xi_z - H_z\xi_x}{J}\right) + \frac{\partial}{\partial\eta}\left(\frac{H_x\eta_z - H_z\eta_x}{J}\right) + \frac{\partial}{\partial\zeta}\left(\frac{H_x\zeta_z - H_z\zeta_x}{J}\right) \tag{41}$$

$$\tilde{P}_3 = \frac{\partial}{\partial\xi}\left(\frac{H_y\xi_x - H_x\xi_y}{J}\right) + \frac{\partial}{\partial\eta}\left(\frac{H_y\eta_x - H_x\eta_y}{J}\right) + \frac{\partial}{\partial\zeta}\left(\frac{H_y\zeta_x - H_x\zeta_y}{J}\right) \tag{42}$$

The diffusion term in general curvilinear coordinates is

$$D^2 = \left(\frac{\tilde{D}}{J} g_{ij}\left(J\tilde{Q}\right)_{,j}\right)_{,i} \tag{43}$$

The metric tensor is defined as

$$g_{ij} = \frac{\partial\bar{x}_i}{\partial\hat{x}_j}\frac{\partial\bar{x}_j}{\partial\hat{x}_i} \tag{44}$$

where $\bar{x}_i$ is the Cartesian coordinate vector and $\hat{x}_i$ is the curvilinear coordinate vector:

$$\bar{x}_i = (x, y, z)^T \qquad \hat{x}_i = (\xi, \eta, \zeta)^T \tag{45}$$

Here, the superscript T represents a transpose. The contravariant components U, V, W of the velocity vector are related to the velocity components u, v, w in the Cartesian system as follows

$$\begin{bmatrix} U \\ V \\ W \end{bmatrix} = \begin{bmatrix} \xi_x & \xi_y & \xi_z \\ \eta_x & \eta_y & \eta_z \\ \zeta_x & \zeta_y & \zeta_z \end{bmatrix} \begin{bmatrix} u \\ v \\ w \end{bmatrix} \tag{46}$$

Similarly, the contravariant components $\hat{H}_\xi$, $\hat{H}_\eta$, $\hat{H}_\zeta$ of the magnetic field vector are defined as

$$\begin{bmatrix} \hat{H}_\xi \\ \hat{H}_\eta \\ \hat{H}_\zeta \end{bmatrix} = \begin{bmatrix} \xi_x & \xi_y & \xi_z \\ \eta_x & \eta_y & \eta_z \\ \zeta_x & \zeta_y & \zeta_z \end{bmatrix} \begin{bmatrix} H_x \\ H_y \\ H_z \end{bmatrix} \tag{47}$$

For the subsystem containing the magnetic field transport equations, the solution vector $\tilde{Q}$, the flux vectors $\tilde{E}$, $\tilde{F}$, $\tilde{G}$, and the source vector $\tilde{S}$ are

$$\tilde{Q} = \frac{1}{J} \begin{bmatrix} H_x \\ H_y \\ H_z \end{bmatrix} \qquad \tilde{E} = \frac{1}{J} \begin{bmatrix} H_x U - u\hat{H}_\xi \\ H_y U - v\hat{H}_\xi \\ H_z U - w\hat{H}_\xi \end{bmatrix} \qquad \tilde{F} = \frac{1}{J} \begin{bmatrix} H_x V - u\hat{H}_\eta \\ H_y V - v\hat{H}_\eta \\ H_z V - w\hat{H}_\eta \end{bmatrix}$$

$$\tilde{G} = \frac{1}{J} \begin{bmatrix} H_x W - u\hat{H}_\zeta \\ H_y W - v\hat{H}_\zeta \\ H_z W - w\hat{H}_\zeta \end{bmatrix} \qquad \tilde{S} = 0 \qquad \tilde{D} = \frac{1}{Rm} I \tag{48}$$

Thus, in the case of three-dimensional magnetohydrodynamics, the system of eight partial differential equations needs to be solved by integrating intermittently a subsystem of five fluid flow equations and a subsystem of three magnetic field transport equations and transferring the information through the source-like terms (Lee, 1990; Lee and Dulikravich, 1991a). The explicit Runge-Kutta time-stepping algorithm and finite difference scheme with artificial compressibility (Chorin, 1967) were used in the general non-orthogonal curvilinear boundary conforming coordinate system. The explicit time integration scheme was used because it can be efficiently vectorized and because additional equations can be easily added to the system. The rate of convergence of explicit schemes is generally much lower than for implicit schemes, but when fully vectorized, these schemes need less central processor unit time to reach the convergence than implicit schemes. This advantage of explicit schemes is more pronounced when three-dimensional problems with complex geometries are studied.

4. COMPUTATIONAL RESULTS

Mathematical and numerical models for solidification of a fluid flow were first tested in the case of a straight two-dimensional channel of aspect ratio 3:1. A uniform non-dimensional temperature $\theta = 1$ was imposed at the inlet. Along the walls a smoothly varying cooling was specified as $\theta = 1 - 11 \sin(\pi x/3)$. Both velocity components were specified at the inlet, while combination of hydrostatic, hydromagnetic and hydrodynamic pressure was specified at the exit. Properties of the fluid flow were defined by the non-dimensional numbers which

are given in Table 1. All physical properties were assumed not to vary with temperature. The flow field was discretized with 60×60 non-clustered grid cells.

The first test case represents a flow field without an externally imposed magnetic field. The computed velocity vector field clearly outlines the solidified zones attached to the channel walls as given in Fig. 1a. Computed streamlines and temperature field are given in Fig. 2a and Fig. 3a. A detail of the flow field adjacent to the bottom wall and immediately downstream of the solidified layer (Fig. 4a) depicts a strong local flow recirculation. Lengths of the vectors in the velocity vector field plots correspond to the magnitudes of the local velocity vectors.

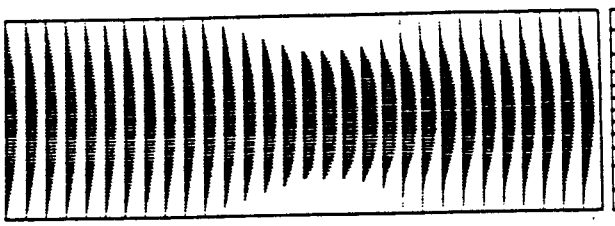

a)

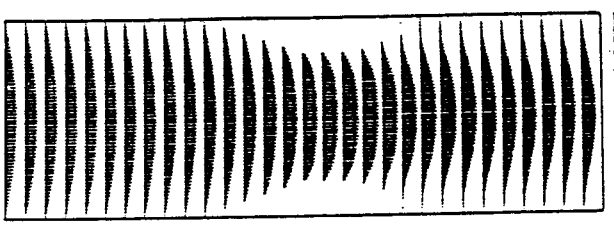

b)

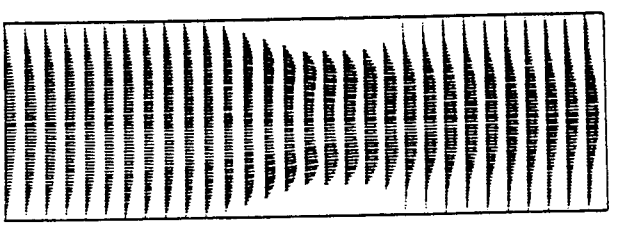

c)

FIGURE 1. Straight channel: velocity vector field; a) test case 1, b) test case 2, c) test case 3.

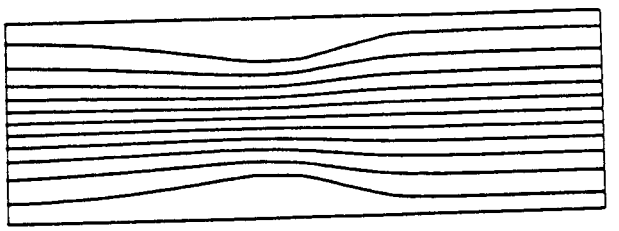

a)

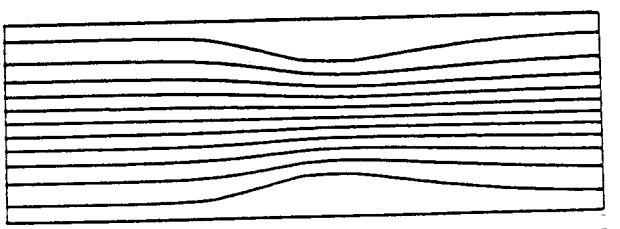

b)

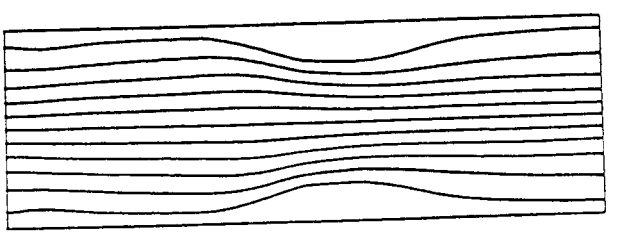

c)

FIGURE 2. Straight channel: streamlines; a) test case 1, b) test case 2, c) test case 3.

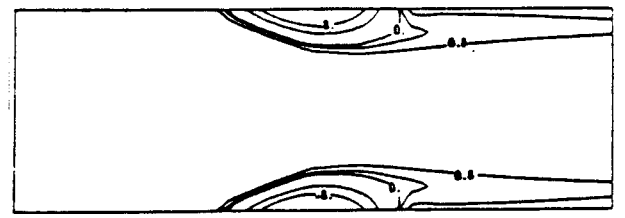

a)

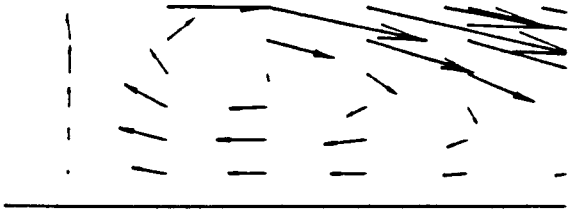

a)

b)

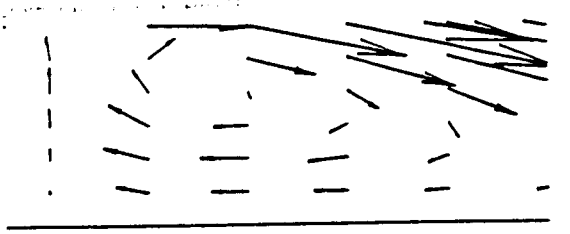

b)

c)

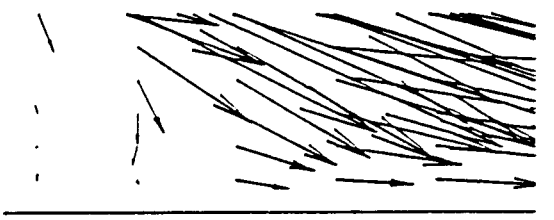

c)

FIGURE 3. Straight channel: isotherms; a) test case 1, b) test case 2 , and c) test case 3.

FIGURE 4. Straight channel: flow recirculation patterns for a) test case 1, b) test case 2, and c) test case 3.

In the second test case the viscosity coefficient was varied throughout the flow field as an arctangent function of the non-dimensional temperature, while in the first test case it varied linearly only within the mushy region. Numbers on isotherm plots (Fig. 3) indicate the values of non-dimensional temperature θ where $\theta = 0$ indicates the solid/liquid interface. No noticeable difference can be seen in the velocity field, streamlines or temperature fields between the second test case (Fig. 1b, Fig. 2b and Fig 3b) and the first test case.

	Straight	U-shaped
Re	100	20
Ec	1	1
Pr	7.9	7.9
Pm	1	1
Ht	5	5 or 10

TABLE 1. Nondimensional Numbers for Straight and U-shaped Channels

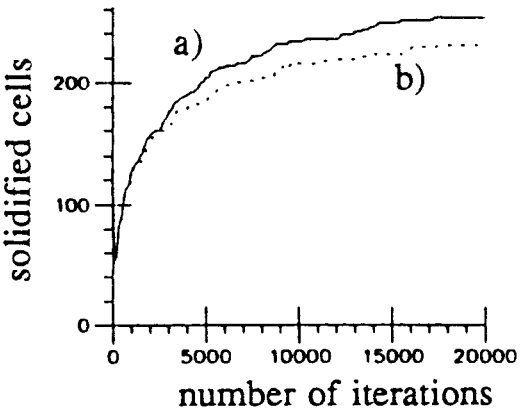

FIGURE 5. Straight channel: convergence histories for a) test case 1, and b) test case 3.

To test the influence of the magnetic field on solidification, a third test run was performed with the viscosity varying linearly in the mushy region and a vertically downward pointing constant magnetic field of Ht = 10. Computed velocity vector field, streamlines, and isotherms are depicted in Figs. 1c, 2c, 3c, respectively. The detail of the computed velocity vector field adjacent to the bottom wall and immediately downstream of the solidified layer (Fig. 4b) demonstrates that the magnetic field is capable of suppressing the flow recirculation caused by the presence of the solidification layers. The convergence history is given in terms of an instantaneous count of the solidified cells in the domain (Fig. 5). It demonstrates that the presence of a magnetic field inhibits the growth of the solid layers because of the higher speed of the fluid next to the solid/fluid interface. This is typical for magnetohydrodynamics.

The next test configuration represented a solidifying flow in a U-shaped channel of constant width. The same type of boundary conditions was imposed on inlet temperature and velocity as in the case of a straight channel. Along the straight parts of the walls the temperature was kept constant ($\theta = 1$). Along the curved parts of the walls the non-dimensional temperature varied according to $\theta = 1 - 11 \sin(\pi/2 - \omega)$ where ω is the angle between the wall point and the horizontal. The computational grid had 264×60 cells that were clustered towards the walls. Non-dimensional numbers used with the U-shaped channel are given in Table 1.

The first test case involved no magnetic field. The computed velocity vector field (Fig. 6a) and streamlines (Fig. 7a) clearly show a large recirculation zone attached to the inner wall immediately following the solidified region depicted in the temperature field plot (Fig. 8a) as $\theta = 0$ value. There was no flow recirculation detected along the outer wall although a sizable solidified layer was predicted there.

In the second test case a uniform magnetic field (Ht = 5) was applied perpendicular to the walls of the entire U-shaped channel. The computed velocity vector field (Fig. 6b) and streamlines (Fig. 7b) demonstrate that the magnetic field effectively eliminates flow recirculation regions. At the beginning of the channel turn we can notice a mild form of the velocity overshoot close to the walls that is characteristic of magnetohydrodynamic flows.

In the third test case a stronger magnetic field (Ht = 10) was applied in the same manner resulting in a dramatic change in the flow pattern (Fig. 6c) due to a strong ponderomotive force, while the differences in the computed streamline pattern (Fig. 7c) and isotherms (Fig. 8c) are less obvious. Convergence histories (Fig. 9) reconfirm an earlier conclusion that the application of a magnetic field inhibits the solidification process because of Joule heating. Plots of the magnetic lines of force for the straight channel (Fig. 10a) and for the U-shaped channel (Fig. 10b) demonstrate their complex patterns that could be exploited to position and orient small particles in the flow field and, consequently, in the solidified layers.

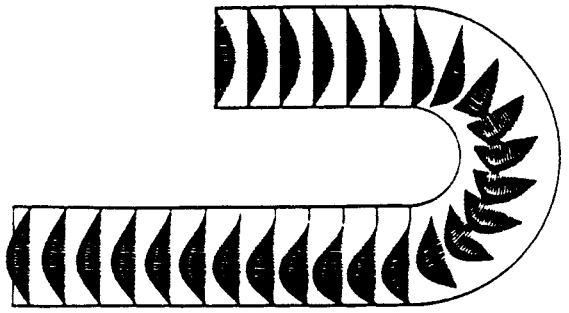

a)

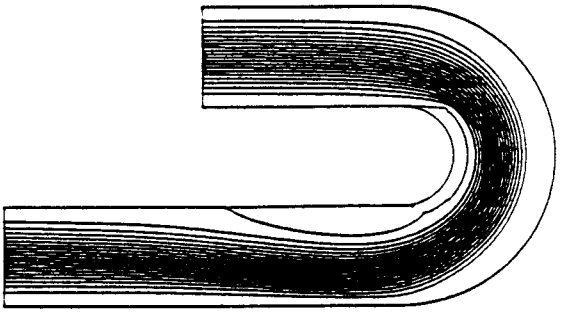

a)

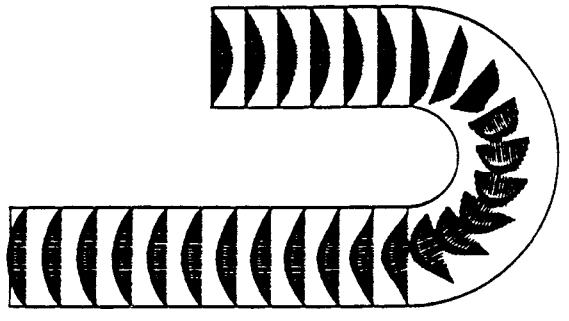

b)

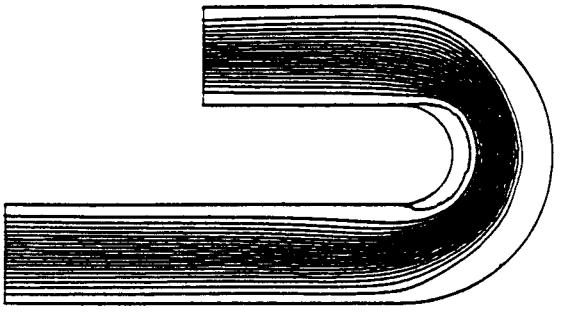

b)

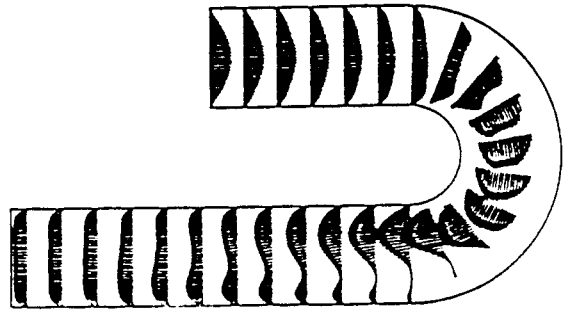

c)

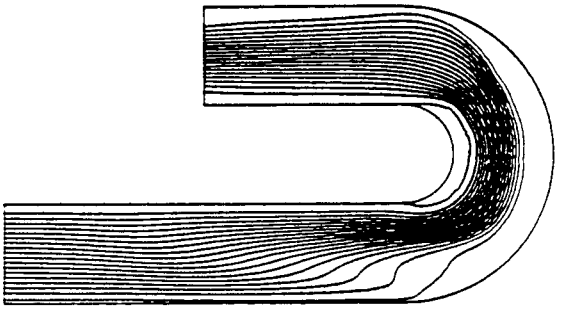

c)

FIGURE 6. U-shaped channel: velocity vector field; a) H_t =0, b) H_t = 5 , c) H_t = 10.

FIGURE 7. U-shaped channel: streamlines; a) H_t =0, b) H_t = 5 , c) H_t = 10.

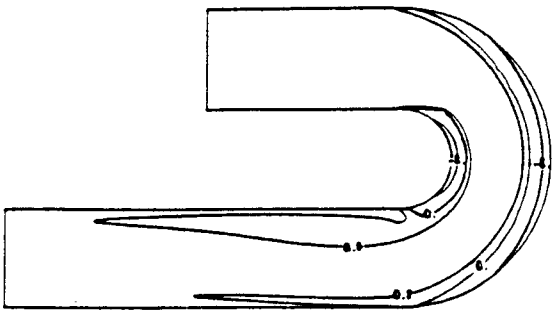

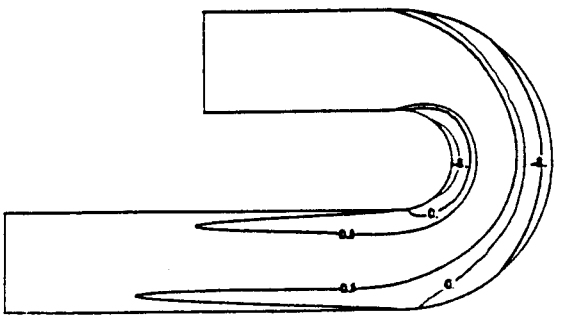

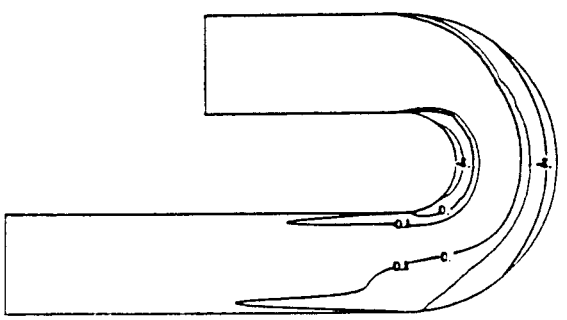

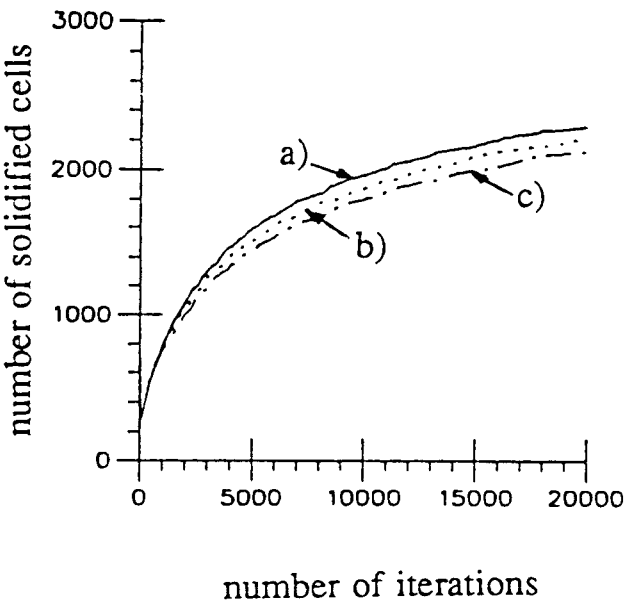

FIGURE 8. U-shaped channel: isotherms; a) $Ha = 0$, b) $Ha = 5$, c) $Ha = 10$.

FIGURE 9. U-shaped channel: convergence histories; a) $Ha = 0$, b) $Ha = 5$, c) $Ha = 10$.

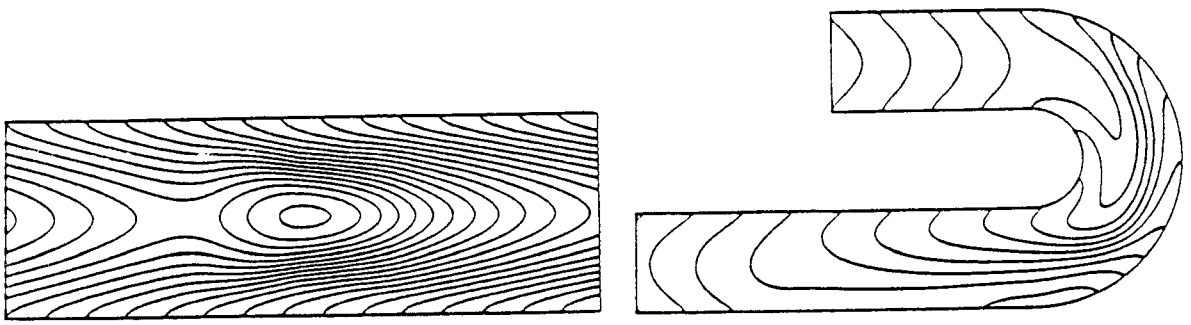

a) b)

FIGURE 10. Magnetic field force lines in solidifying channel flows with Ht = 10: a) straight channel , and b) U-shaped channel.

Finally, the mathematical model and the computer code were tested using a set of realistic physical flow parameters corresponding to a blood flow in an arbitrary shaped channel with undercooled walls. The values of physical properties for blood (Fazzio and Jacobs, 1974; Balasubramaniam and Bowman, 1977; Sud, Sekhon and Mishra, 1977; Diller, 1985) are given in Table 2. As in previous two test configurations, the temperature of the walls from inlet to exit was varying according to a sinusoidal distribution $\theta = 1 - 11 \sin(\pi\, i / imax)$ where i is the grid cell index in the x-direction ($1 < i < imax$). Fluid temperature at the inlet was a uniform T = 283 K corresponding to $\theta = 1$ since $T_h = 283$ K and $T_c = 273$ K so that $\Delta T_o = T_h - T_c = 10$ K. This made the coldest point on the wall have a temperature of -100 degrees Celsius. In the case when a steady uniform magnetic field was applied, it acted vertically downward between the inlet and the 80% of the channel length, while no magnetic field was applied over the remaining 20% of the channel length. The characteristic quantities that were used for non-dimensionalization are: $c_{po} = c_{pol}$, $k_o = k_{ol}$, $l_o = 0.01$ m , $v_o = 0.1$ m/s. Since the value for the magnetic permeability for blood could not be found in the open literature, we have assumed it to be $\mu = 50\ \mu_v$, where $\mu_v = 4\ \pi \times 10^{-7}$ is the magnetic permeability for vacuum. If $B_0 = \mu_v\ H_0$, the remaining terms in the equation (13) for Ht can be grouped so that Ht is directly proportional to B_0 which is measured in Teslas. For example, if $Ht = 0.5\ B_0$ and the value for B_0 is 10, this means that the Hartmann number Ht = 5 can be achieved with the magnetic field of 10 T. The non-dimensional numbers used in the simulation of freezing of blood flow are given in Table 3.

It should also be pointed out that the correct value for the magnetic Prandtl number was not used because it was extremely small and caused the initial residuals in the iterative process to diverge. Instead, we have used a value for the P_m which is ten orders of magnitude larger.

The non-orthogonal boundary-conforming computational grid consisted of 100x58 grid cells that were clustered towards the inlet and the passage top and bottom walls. The grid was generated using our grid optimization algorithm (Kennon and Dulikravich, 1986).

A comparison of the computational results with and without an external magnetic field shows that the velocity profiles change under the influence of the magnetic field due to the ponderomotive force (Figs. 11a and 11b). More importantly, the solidified layers in the case where no external magnetic field was applied are thicker and differently shaped compared to the freezing with the magnetic field. It can be seen from the plots of streamlines (Figs. 12a and 12b) and isotherm plots (Fig. 13a and 13b).

ρ_o [kg m^{-3}]	1055
C_{pol} [J kg^{-1} K^{-1}]	4184
C_{pos} [J kg^{-1} K^{-1}]	2080
k_{ol} [W m^{-1} K^{-1}]	0.51
k_{os} [W m^{-1} K^{-1}]	0.183
T_l [K]	273.5
T_s [K]	273
η_o [kg m^{-1} s^{-1})]	4.5 x 10^{-3}
α [K^{-1}]	1 x 10^{-4}
L [J kg^{-1}]	300000
σ [Ω^{-1} m^{-1}]	0.005

TABLE 2. Physical Properties for Blood.

Re	234.44
Ec	6.46 x 10^{-8}
Pr	36.9
Pm	2.68 x 10^{-3}
Ht	.5027 B_o

TABLE 3. Non-dimensional Numbers for Blood

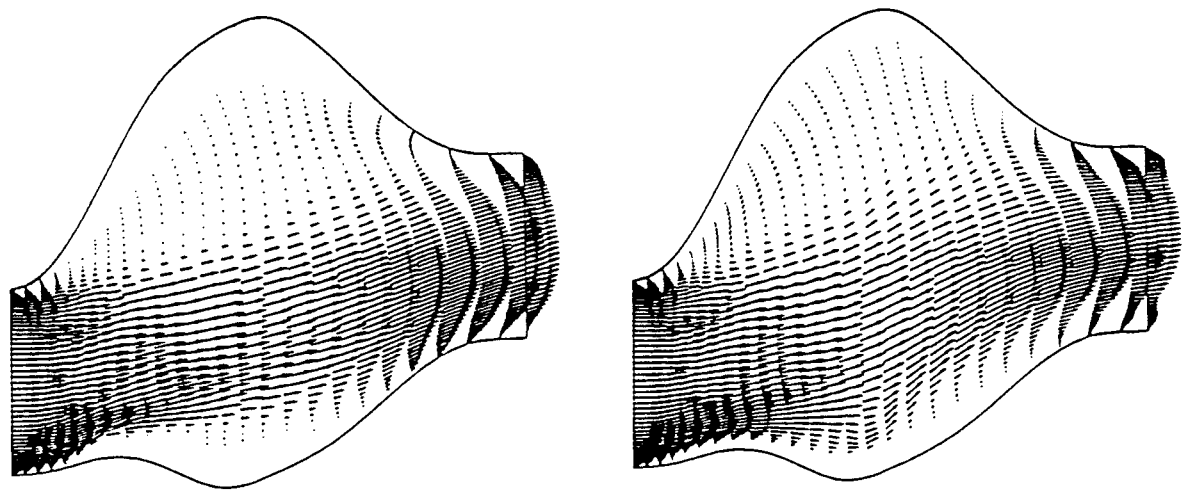

a) b)

FIGURE 11. Velocity vector fields for a steady flow with solidification inside an arbitrary two-dimensional channel: a) no magnetic field, and b) magnetic field with $B_0 = \mu_v H_0 = 10$ T.

The change of velocity profile next to the solid/liquid interface causes the change in the convective heat transfer. In this case as well as in the previous cases Joule heating effects are relatively negligible. The difference in the number of solidified cells with and without the magnetic field can be seen from the convergence histories (Fig. 14) of the two test cases.

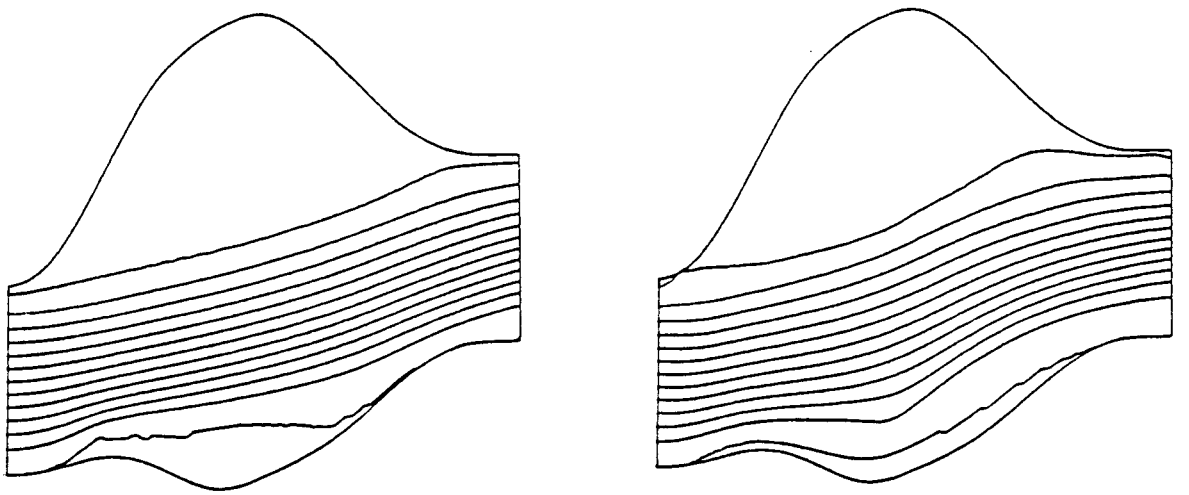

a) b)

FIGURE 12. Streamlines for a steady flow with solidification inside an arbitrary two-dimensional channel: a) no magnetic field, and b) magnetic field with $B_0 = \mu_v H_0 = 10$ T.

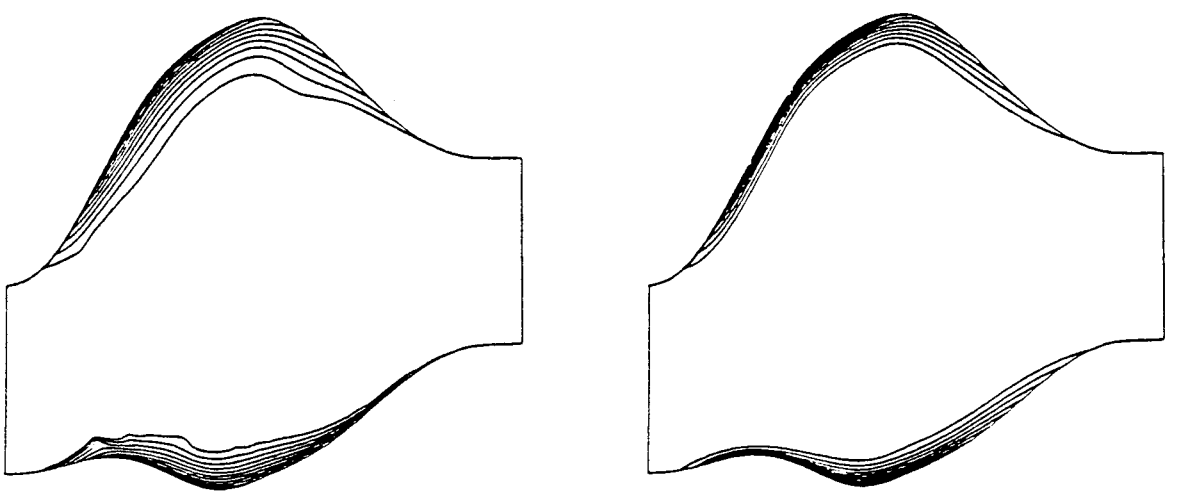

a) b)

FIGURE 13. Isotherms for a steady flow with solidification inside an arbitrary two-dimensional channel: a) no magnetic field, and b) magnetic field with $B_0 = \mu_v H_0 = 10$ T.

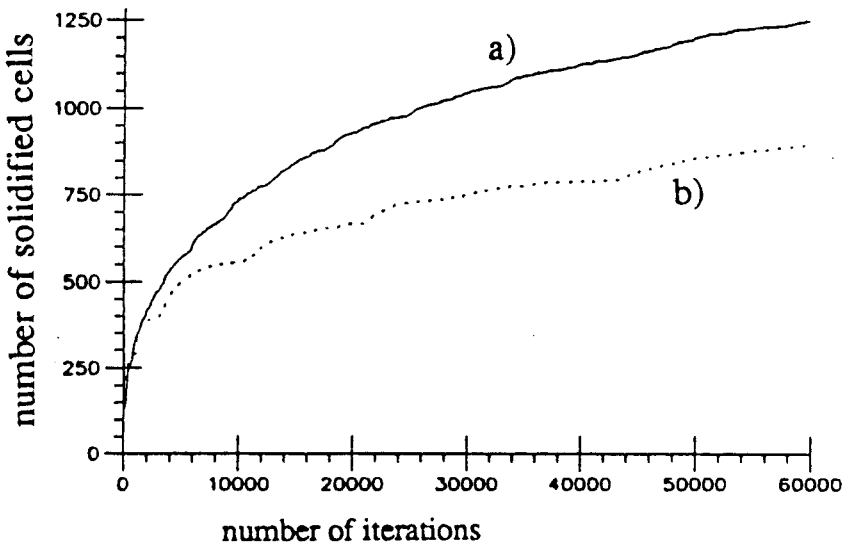

FIGURE 14. Convergence histories for a steady flow with solidification inside an arbitrary two-dimensional channel: a) no magnetic field, and b) magnetic field with $B_0 = \mu_v H_0 = 10$ T.

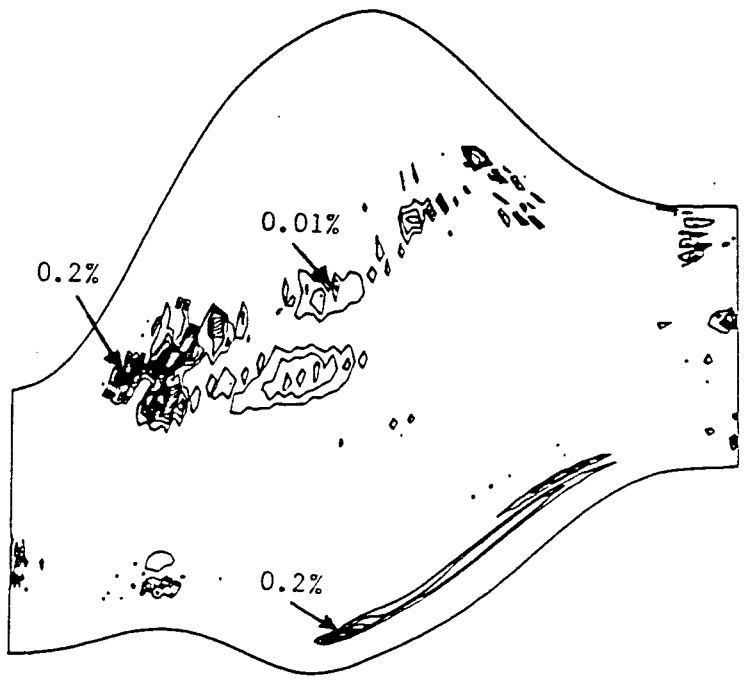

FIGURE 15. Lines of constant Joule heating for a steady blood flow with solidification inside an arbitrary two-dimensional passage with a magnetic field $B_0 = \mu_v H_0 = 10$ T.

From Figure 15 it can be concluded that the Joule heating effect is negligible (less than one percent of the latent heat) in influencing the solidification process for the values of the parameters used in this test case. It is the higher speed of the fluid close to the solid/liquid interface that decreases the residence time of the fluid particles in the mushy region, thus decreasing the rate of solid accretion. This increase in the fluid speed in the boundary layer regions is caused by the presence of the magnetic field. On the other hand, Joule heating would have a profound influence on the solidification rate in the case of a lower electrical conductivity of the fluid and in flows generated purely by thermal buoyancy.

5. CONCLUSIONS

A complete analytical and numerical formulation has been developed for the theoretical prediction of solidification processes in fluid flows inside undercooled passages with and without the influence of an externally applied steady magnetic field. Computational results confirm that the magnetic field has a profound influence on the solidifying flow field since it eliminates flow recirculation regions and causes distorted velocity profiles having pronounced overshoots close to the solid boundaries. Temperature field also changes under the influence of the external magnetic field. This change influences heat transfer through the boundaries and consequently the amount of the solid phase accrued on undercooled walls. Specifically, the influence of the ponderomotive force and, to a much lesser extent, Joule heating are such that they tend to reduce the amount of the accrued solid phase. Combined with the predicted complex patterns of the magnetic field force lines, this indicates a possibility for the development of a computational optimization algorithm capable of achieving desired configurations of the solidifyed layers and desired distribution of non-reactive particles within the solidifyed layers.

ACKNOWLEDGMENTS

The authors would like to express their gratitude to Mr. Scott G. Sheffer for his help in the preparation of this paper. All computations were performed remotely on the Cray-YMP computer at NASA Ames Research Center NAS facility and at Cray Research, Inc. in Eagan, Minnesota and post processed on the equipment donated by Apple Computer, Inc.

6. REFERENCES

Balasubramaniam, T.A. and Bowman, H.F., Thermal Conductivity and Thermal Diffusivity of Biomaterials: A Simultaneous Measurement Technique, *Journal of Biomedical Engineering*, August 1977, pp. 148-154.

Chandrasekhar, S., *Hydrodynamic and Hydromagnetic Stability*, Dover Publication Inc., New York, 1961.

Chorin, A. J., A Numerical Method for Solving Incompressible Viscous Flow Problems, *Journal of Computational Physics*, Vol. 2, 1967, pp. 12-26.

Diller, K. R., The Influence of Controlled Ice Nucleation on Regulating the Thermal History During Freezing, *Cryobiology*, Vol.22, 1985, pp.268-281.

Dulikravich, G. S. and Hayes, L. J., Control of Surface Temperatures to Optimize Survival in Cryopreservation, Proc. of ASME WAM '88 *Symposium on Computational Methods in Bioengineering*, ed. R. L. Spilker and B. R. Simon, Chicago, IL, Nov. 27-Dec.2, 1988, BED-9, pp. 255-265.

Dulikravich, G. S., Kosovic, B. and Lee, S., Solidification of Variable Property Melts in Closed Containers: Magnetic Field Effects, Proc. 13th IMACS World Congress on Computation and Applied Math., Dublin, Ireland, July 22-26, 1991.

Fazzio, R.G. and Jacobs, H.R., Heat Transfer Coefficients of Blood in Small Tubes and Capillaries, *AIChE Symposium Series*, 138, Vol.70, 1974, pp. 233-240.

Gray, D. D., and Giorgini, A., The Validity of the Bousinessq Approximation for Liquids and Gases, *International Journal of Heat and Mass Transfer*, Vol. 19, 1976, pp. 545-551.

Heiser, W. H., Influence of Magnetic Fields Upon Separation, *AIAA Journal*, Vol. 2, No. 12, 1964, pp. 2217-2218.

Ievlev, V. M. and Levin, V. B., Laminarization of a Submerged Jet of Electrically Conducting Fluid by Means of a Longitudinal Magnetic Field, *Izvestia Academii Nauk SSSR, Mekhanika Zhidkosti i Gaza,* No. 6, Nov-Dec. 1989, pp. 35-40.

Jameson, A., Schmidt, W. and Turkel, E., Numerical Solution of the Euler Equations by Finite Volume Methods Using Runge-Kutta Time-Stepping Scheme, AIAA paper 81-1259, AIAA Computational Fluid Dynamics Conference, Palo Alto, CA, June 1981.

Jeffrey, A., Magnetohydrodynamics, University Mathematical Texts 33, Oliver & Royd LTD., Edinburgh, U.K, 1966.

Kennon, S.R. and Dulikravich, G.S., Optimization of Computational Grids, *AIAA Journal,* Vol.24, No. 7, July 1986, pp.1069-1073.

Lee, S. and Dulikravich, G. S., Magnetohydrodynamic Steady Flow Computations in Three Dimensions, AIAA Paper 91-0388, AIAA Aerospace Sciences Meeting, Reno, NV, Jan. 1991a; also *International Journal for Numerical Methods in Fluids,* Vol. 13, No. 8, 1991a.

Lee, S. and Dulikravich, G. S., Computation of Magnetohydrodynamic Flow With Joule Heating and Buoyancy, Proceedings of International Aerospace Congress, Melbourne, Australia, May 13-17, 1991b.

Lee, S. and Dulikravich, G.S., Performance Analysis of DMR Method for Acceleration of Iterative Algorithms, AIAA paper 91-0241, AIAA Aerospace Sciences Meeting, Reno, NV, Jan. 7-10, 1991c.

Lee, S., Dulikravich, G. S. and Kosovic, B., Interaction of a Magnetic Field with Blood Flow, Proc. 17th Annual Northeast Bioengineering Conference, University of Connecticut, Hartford, CT, April 4-5, 1991a.

Lee, S., Dulikravich, G. S. and Kosovic, B., Electrohydrodynamic (EHD) Flow Modeling and Computations, AIAA paper 91-1469, AIAA Plasma Physics, Fluid Dynamics and Lasers Conference, Honolulu, Hawaii, June 24-26, 1991b.

Ozoe, H. and Okada, K., The Effect of the Direction of the External Magnetic Field on the Three-Dimensional Natural Convection in a Cubical Enclosure, *International Journal of Heat and Mass Transfer,* Vol. 32, No. 2, 1989, pp. 1939-1954.

Pai, S.-I., *Magnetogasdynamics and Plasma Dynamics,* Springer Verlag, Vienna, 1962.
Stuetzer, O. M., Magnetohydrodynamics and Electrohydrodynamics, *The Physics of Fluids,* Vol. 5, No. 5, May 1962, pp. 534-544.

Sud,V.K., Sekhon, G.S. and Mishra, R.K., Pumping Action of Blood by a Magnetic Field, *Bulletin of Mathematical Biology,* Vol. 39, 1977, pp.385-390.

Vives, C., Effects of a Magnetically Forced Convection During the Crystallization in Mould of Aluminum Alloys, *Journal of Crystal Growth,* Vol. 94, 1989, pp. 739-750.